Journal of Innovative Optical Health Sciences
Vol. 11, No. 5 (2018) 1850032 (12 pages)
© The Author(s)
DOI: 10.1142/S1793545818500323

In vivo monitoring of microneedle-based transdermal drug delivery of insulin

Jiawei Zhao[*,‡], Yongbo Wu[*,§], Junbo Chen[*,¶], Bangrong Lu[*,‖],
Honglian Xiong[†,**], Zhilie Tang[*,††,§§] and Yanhong Ji[*,‡‡,§§]
[*]*School of Physics and Telecom Engineering*
South China Normal University, No.378 West Waihuan Street
Guangzhou 510006, P. R. China

[†]*MOE Key Laboratory of Laser Life Science*
and Institute of Laser Life Science
College of Biophotonics, South China Normal University
No.55 Zhongshan Xi Road, Guangzhou 510631, P. R. China
[‡]*2015020896@m.scnu.edu.cn*
[§]*wuyongbo@m.scnu.edu.cn*
[¶]*2015020894@m.scnu.edu.cn*
[‖]*768306878@qq.com*
[**]*yuanxiufeng138@163.com*
[††]*tangzhl@scnu.edu.cn*
[‡‡]*jiyh@scnu.edu.cn*

Received 6 June 2018
Accepted 5 August 2018
Published 12 September 2018

Soluble microneedles (MNs) have recently become an efficient and minimally invasive tool in transdermal drug delivery because of their excellent biocompatibility and rapid dissolution. However, direct monitoring of structural and functional changes of MNs *in vivo* to estimate the efficiency of insulin delivery is difficult. We monitored the dissolution of MNs to obtain structural imaging of MNs' changes by using optical coherence tomography (OCT). We also observed the effect of MNs on microvascular conditions with laser speckle contrast imaging (LSCI) and measured the blood perfusion of skin to obtain functional imaging of MNs. We determined the performance of two soluble MN arrays made from polyvinyl alcohol (PVA) and polyvinyl alcohol/polyvinylpyrolidone (PVA/PVP) by calculating the cross-sectional areas of the microchannels in mouse skin as a function of time. Moreover, the change in blood glucose before and after using MNs loaded with insulin was evaluated as an auxiliary means to demonstrate the ability of the soluble MNs to deliver insulin. Results showed that the structural imaging of these MNs could be observed *in vivo* via OCT in real time and the functional imaging of MNs could be

---

[§§] Corresponding authors.

showed using LSCI. OCT and LSCI are potential tools in monitoring MNs structural and functional changes.

Keywords: Soluble microneedle; insulin; optical coherence tomography; laser speckle contrast imaging.

1. Introduction

Diabetes is a group of metabolic diseases characterized by high blood glucose level. Diabetics are apt to develop blindness, kidney disease and heart disease.[1] Although diabetes is not an infectious disease, it spreads rapidly at an increasing rate and is now considered a pandemic; thus, developing a therapy that realizes glycemic targets is important. With the development of drug delivery systems, insulin may be administered via various routes, such as oral,[2] parenteral[3] and transdermal routes.[4] Each improvement in drug delivery aims to ensure patient convenience and enhance glycemic control.

Transdermal drug delivery has widely been used given its being noninvasive and patient friendly. Traditional transdermal drug delivery systems include creams, ointments and transdermal patches. However, stratum corneum (SC) layer, which is the principal barrier to topically applied drugs, restricts the translocation of drugs into deeper skin layer.[5] The SC allows only a small number of low-molecular-weight drugs (< 500 Daltons) to pass through the skin.[6] To overcome the skin barrier property and allow transdermal penetration of a large range of molecules, including biological macromolecules (e.g., proteins,[7] DNA,[8] vaccines,[9] or other therapeutic drugs), researchers have recently developed microneedles (MNs). MNs are a drug delivery system that is an intermediate form of hypodermic needle and transdermal patch; MNs create a number of transdermal microchannels on the skin and pierce through the SC to increase drug permeability.[10] MNs are made of silicon,[11] metal,[12] or polymers.[13] Compared with metal and silicon MNs, biodegradable MNs enhance the efficiency of transdermal delivery and avoid needles from being stuck in the skin.[14] Specifically, soluble polymer MNs produced from polyvinyl alcohol (PVA), polyvinylpyrolidone (PVP).[15,16] silk fibroin,[17] or carboxymethyl cellulose[18] rapidly dissolve when they come in contact with water. Thus, when they puncture the skin, a drug loaded into the needles is delivered into the skin as the needles dissolve. Numerous soluble MN application systems for transdermal delivery of insulin have been developed,[19,20] such as composite microneedles integrated with insulin-loaded $CaCO_3$ microparticles and PVP,[21] microneedles fabricated from alginate and maltose[22] and near-infrared light triggered and separable microneedles.[23,24] Insulin regulates glucose levels in normal circumstances; thus, monitoring the release and the efficiency of insulin delivery is important.

Several optical imaging technologies have been used to monitor the effects of MNs applied on the skin. These technologies include two photon microscopy,[25] confocal laser fluorescence microscopy[26] and optical coherence tomography (OCT).[27–29] The confocal microscopy can only observe the effect of MNs on isolated skin tissue. Two-photon microscopy and confocal laser fluorescence microscopy can investigate the delivery of fluorescent drugs which is wrapped in the MNs. It is not appropriate for most colorless drugs like insulin. Compared with other optical imaging technologies, OCT achieves a larger imaging depth of 2–3 mm and a high resolution at the micrometer scale. It is a noninvasive interferometric technique. This technique is appropriate in evaluating the efficiency of nonfluorescent drug transdermal delivery *in vivo*[30,31] So OCT is a potential tool in structural imaging of MNs changes *in vivo*. Compared with other teams that used OCT to monitor MNs changes *in vivo*, we introduced cross-sectional area of the microchannels and the slop to quantitatively evaluate the dissolution of the MN arrays. Besides, we estimated and compared the different dissolution ability of two kinds of MNs in the skin.

Although *in vivo* monitoring of the change of soluble MNs by OCT has been reported, functional imaging of MNs changes *in vivo* is rarely reported. In this paper, in addition to the structural imaging of the MNs changes *in vivo* by OCT, we also have a functional imaging of it with LSCI for the first time. LSCI is a noninvasive and continuous method for measuring microvascular blood flow. This technique which was first introduced in the 1980s can be used to provide two-dimensional (2D) image of blood flow in biological tissue with a high spatial and temporal resolution.[32] It has been widely used because of its simplicity, real-time feedback, and negligible motion artifacts.[33]

In this work, we fabricated two kinds of polymer MNs displaying different dissolution rates. Both MNs loaded with insulin were used for transdermal delivery in rat skin. We built an OCT system to observe the morphological changes of MNs with time and monitored the effect of MNs on microcirculation with LSCI. Additionally, we evaluated the changes in blood glucose before and after the application of insulin-loaded MNs. And then we estimated and compared the different dissolution ability of MNs in the skin.

2. Materials and Methods

2.1. *Fabrication of MNs*

Figure 1 shows the schematic of the fabrication of soluble MNs. A commercial metal MN patch for a beauty product was used as a master mold for the soluble MN arrays. The metal MNs on the array were 500 μm high consisting of 36 needles in a 10 mm × 10 mm area. In making the molds, PDMS solution (Sylgard 184, Dow Corning) was prepared by mixing an elastomer and a curing agent in a 10:1 w/w ratio and then placed in a vacuum oven at −80 kPa until bubbles were removed. These master structure arrays were coated with the treated PDMS and cured for 12 h at 40°C or 2 h at 80°C. The master mold was carefully peeled off from the PDMS mold and saved for reuse.

After manufacturing the PDMS molds, we chose PVA (1799, Aladdin) or PVA:PVP (K13–18, Aladdin) at 4:1 ratio as materials for fabricating the MN arrays. Pure PVA or PVA/PVP was dissolved in deionized water at 15% concentration and heated at 95°C for 2 h for complete dissolution. The PVA or PVA/PVP solution was set aside overnight until clear. Insulin (5 mg; obtained from bovine pancreas, Aladdin, $\geq$ 27 IU/mg, MW 5733.49) was dissolved in PBS (1 ml; pH = 2) to prepare an insulin solution that will serve as model drug. The insulin solution was poured into the PDMS mold, which was subsequently placed in a vacuum oven at −80 kPa to induce the solution to flow into the mold. After the liquid was pipetted onto the surface of PDMS mold and after desiccation, the 15% (w/v) PVA or PVA/PVP solution was poured into the PDMS mold, which was placed in a vacuum oven at −85 kPa for 5 min to remove entrapped bubbles and to better allow the solution melt to set into the mold. After drying overnight, the PVA or PVA/PVP needles were removed from the PDMS mold by using an adhesive tape (Fig. 1). The final MN arrays were stored in a desiccated container for future use.[34]

2.2. *Animals*

Adult balb/c mice of approximately 25–36 g in weight were used in the experiments. The mice

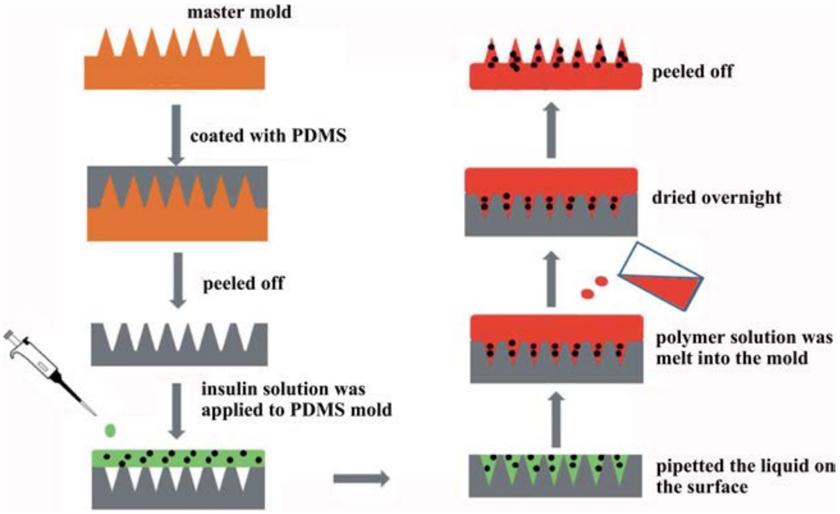

Fig. 1. Fabrication of dissolving microneedles.

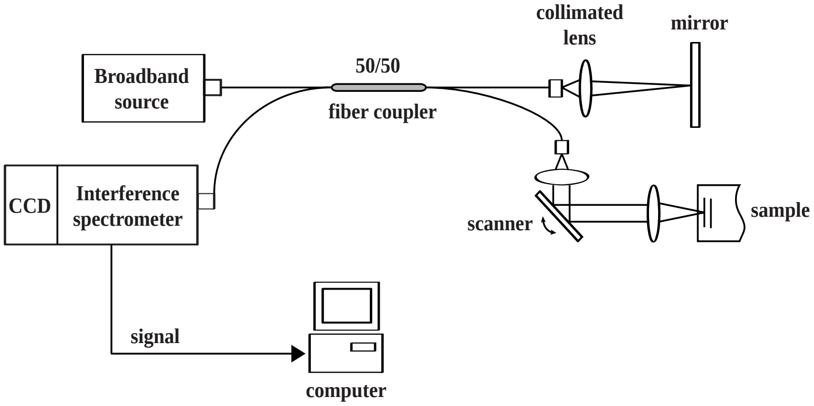

Fig. 2. Schematic of the SD-OCT system.

were anesthetized via peritoneal injection of 1% pentobarbital sodium (60–80 mg/kg). Their ears were de-haired through smearing with hair removal cream. The mice were subsequently placed on a fixed platform to reduce vibration and movement.

2.3. *OCT system*

A homemade spectral-domain OCT (SD-OCT) system was set up for experimentation (Fig. 2). In this system, a low-coherence broadband light source (DL-BX9-CS3307A, dense light) with a central wavelength of 1310 nm and a bandwidth of 58 nm was split into reference arms and sample arms by a fiber coupler with a coupling coefficient of 50/50. The reflected and backscattered light from the reference and sample arms were interfered in the fiber coupler. The signal was detected by CCD (SU1024-LDH2) after splitting the interference light into different wave vectors in the interference spectrometer by using a transmission grating (1004-2, 1145 l/mm). A high-speed scanner (GVS002-2D, Thorlabs) in the sample arms was used to obtain lateral scanning by moving the mirror relative to the sample. The signal and data were transmitted to a computer for data processing.[35,36] This OCT system provides an axial resolution of approximately 15 μm and a transverse resolution of approximately 18 μm as determined by the focal spot size produced by the probe beam. The imaging depth of this system is approximately 2 mm, and the lateral scanning length is approximately 4 mm. Thus, the 2D OCT images are 2 mm × 4 mm (500 × 1024 pixels).

2.4. *Evaluation of microvascular reactivity with LSCI*

We used a laser speckle contrast imager (SQRay, China) to measure the perfusion in the skin of mouse ear. A coherent laser light with a wavelength of 785 nm illuminates the tissue and generates the random speckle pattern. The movements of moving scattering particles in the tissue generate dynamic speckle images which are recorded by the CCD. After averaging the speckle pattern over the finite exposure time of the camera, the image becomes blurred. The degree of blurring is denoted by speckle contrast. Speckle contrast is defined as the ratio of the standard deviation of the intensity to the mean of the intensity in the speckle pattern.[37] As the speckle contrast and the scatter flow velocity are related inversely, blood vessels can separate from the background. So we can get a 2D perfusion image. The image acquisition rate was 20 frame/s and the measurement distance is approximately 30 cm. We collected LSCI images of the microvascular every 5 minutes after inserting MN in the skin and removing it. The mean perfusion level (the flow of blood to the body's organs per unit time) of the interest region was calculated by the software and stored on a computer.

2.5. *Measurement of blood glucose in mouse*

The balb/c mice were fasted for 6 h prior to the experiment. We divided them into four groups: (1) control group, which was not administrated with any drug; (2) PVA MN group, which was administrated with two patches of insulin-loaded MNs applied on the skin of the ears; (3) PVA/PVP MN group, which was administrated with two patches of insulin-loaded MNs applied on the skin of the ears; (4) IP group, which was administered with insulin solution injected intraperitoneally by using a syringe needle. All of them were anesthetized and shaved as described previously. Blood samples were collected from the tail vein. Blood glucose levels were measured by a glucometer (ONETOUCH, SelectSimple) every 30 mins for 4 h after drug administration. The percentage change in blood glucose levels was calculated based on the initial levels at each time interval.

3. Result and Discussion

3.1. *Imaging of the MN array structure*

For the purposes of visualization, we loaded the soluble MN arrays with calcein in the manner described above. Calcein emits a fluorescence. As shown in Fig. 3(a), calcein was successfully loaded into the soluble MN arrays. In addition, OCT was used to observe the 3D morphologies of MNs (Fig. 3(b)).

3.2. *Structural image of the dissolution of MN arrays by OCT*

In the experiment, we collected images every 10 min for 4 h. In this paper, we show the OCT images obtained every 30 min. Figures 4 and 5 show the OCT images of the dissolution of PVA MN arrays and PVA/PVP MN arrays, respectively. After inserting the patches into the mouse ear, the MN arrays dissolved over time. Figures 4(j) and 5(j) show the intact skin before insertion of the patches. Figures 4(k) and 5(k) show the morphology of the skin after patch removal as imaged by OCT. As shown in Figs. 4(a) and 5(a), microchannels were created because of the penetration of the patches. Moreover, a small indentation was created after the patches were removed (indicated by yellow arrows in Figs. 4(k) and 5(k)). The microchannels became narrower, shorter, smaller, or even disappeared as the MN arrays gradually dissolved. Comparison of the images in Figs. 4 and 5 shows that the diameters and depths of the microchannels created by the PVA MN arrays became smaller and shorter. By contrast, the microchannels created by the PVA/PVP MN arrays nearly disappeared.

To quantitatively evaluate the dissolution of the MN arrays, we calculated the cross-sectional area of the microchannels on the mouse skin. The microchannels are indicated by red rows in Figs. 4(a) and 5(a). Figure 6(a) shows the estimated change in cross-sectional area over time after insertion of the PVA or PVA/PVP MN arrays into the skin. We used the slop of Fig. 6(a) to indicate the dissolution rate of MNs (Fig. 6(b)). The experimental results demonstrate that the cross-sectional areas decreased with time because of the dissolution of the MN arrays. PVA MN arrays rapidly dissolved before 60 mins. Beyond 60 mins, their dissolution rate decreased. As for the PVA/PVA MN arrays, the reduction in their dissolution rates was relatively uniform. However, they dissolved slightly faster within the first half hour. Moreover, their dissolution rate decreased faster than that of the PVA MN arrays within 30 mins. Therefore, OCT can directly detect the dissolution of MN arrays and can quantitatively evaluate the dissolution MN arrays in the

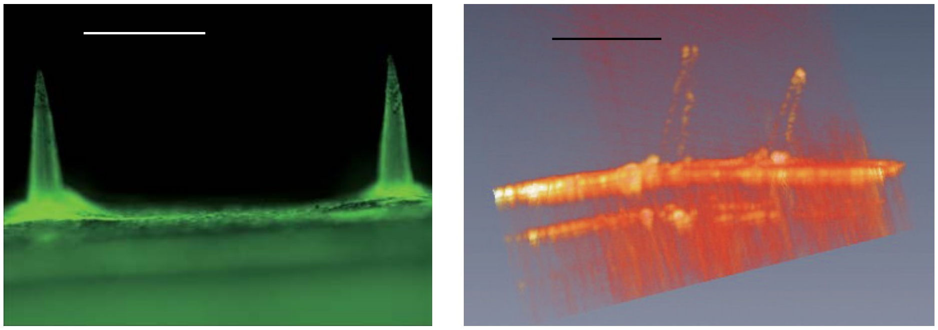
(a) (b)

Fig. 3. (a) Fluorescence micrograph of MN arrays loaded with calcein and (b) 3D image of OCT. The scale bar in (a)(b) represents 0.5 mm in length.

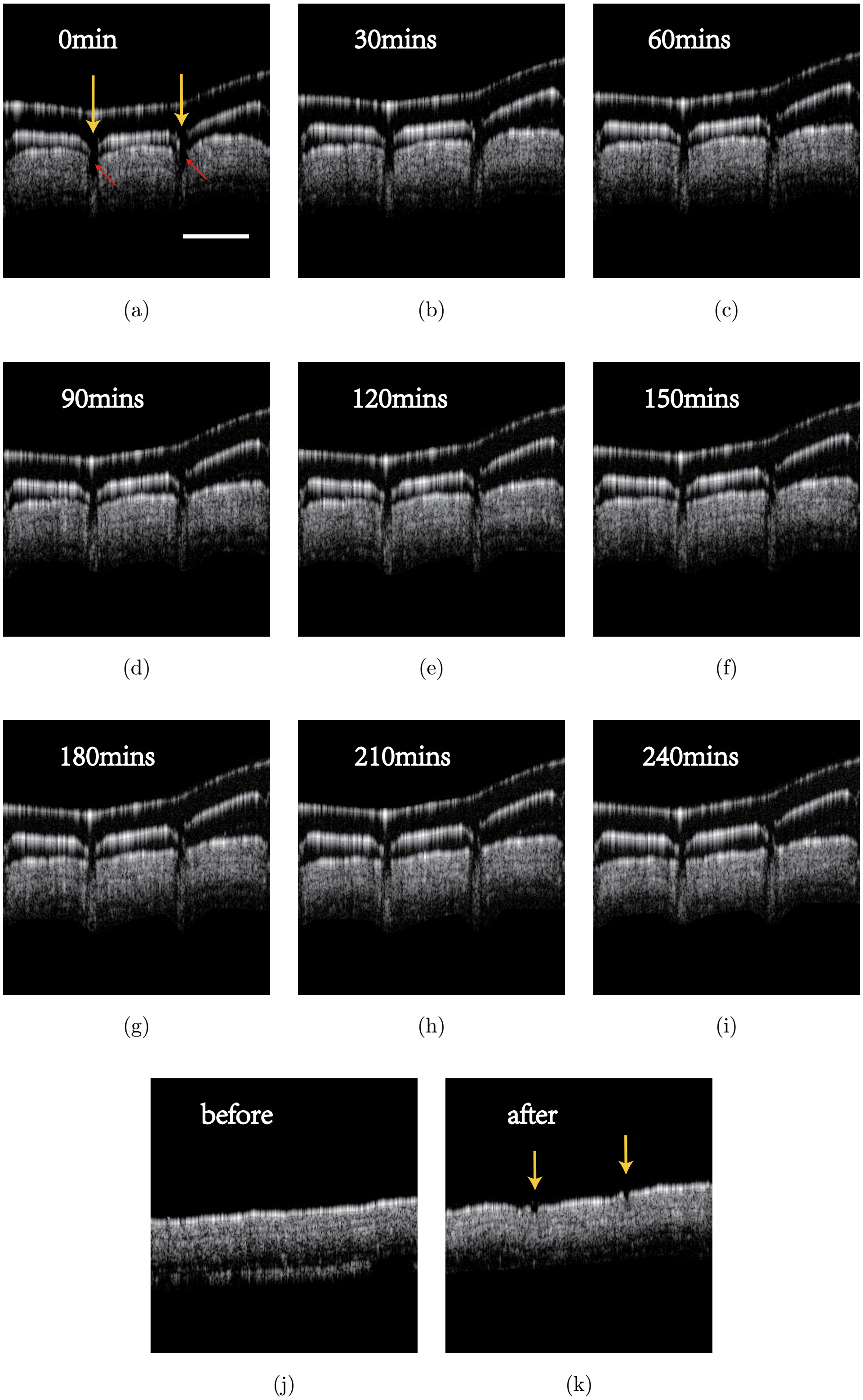

(a) (b) (c)

(d) (e) (f)

(g) (h) (i)

(j) (k)

Fig. 4. OCT images of the dissolving process of PVA MNs on mouse ear (j) before inserting the microneedle patch on the skin: (a) 0 min, (b) 30 mins, (c) 60 mins, (d) 90 mins, (e) 120 mins, (f) 150 mins, (g) 180 mins, (h) 210 mins, (i) 240 mins and (k) after removing the MN patch. The scale bar and the yellow arrow in (a) represent 1 mm in length and the location where the microneedle is inserted into the skin.

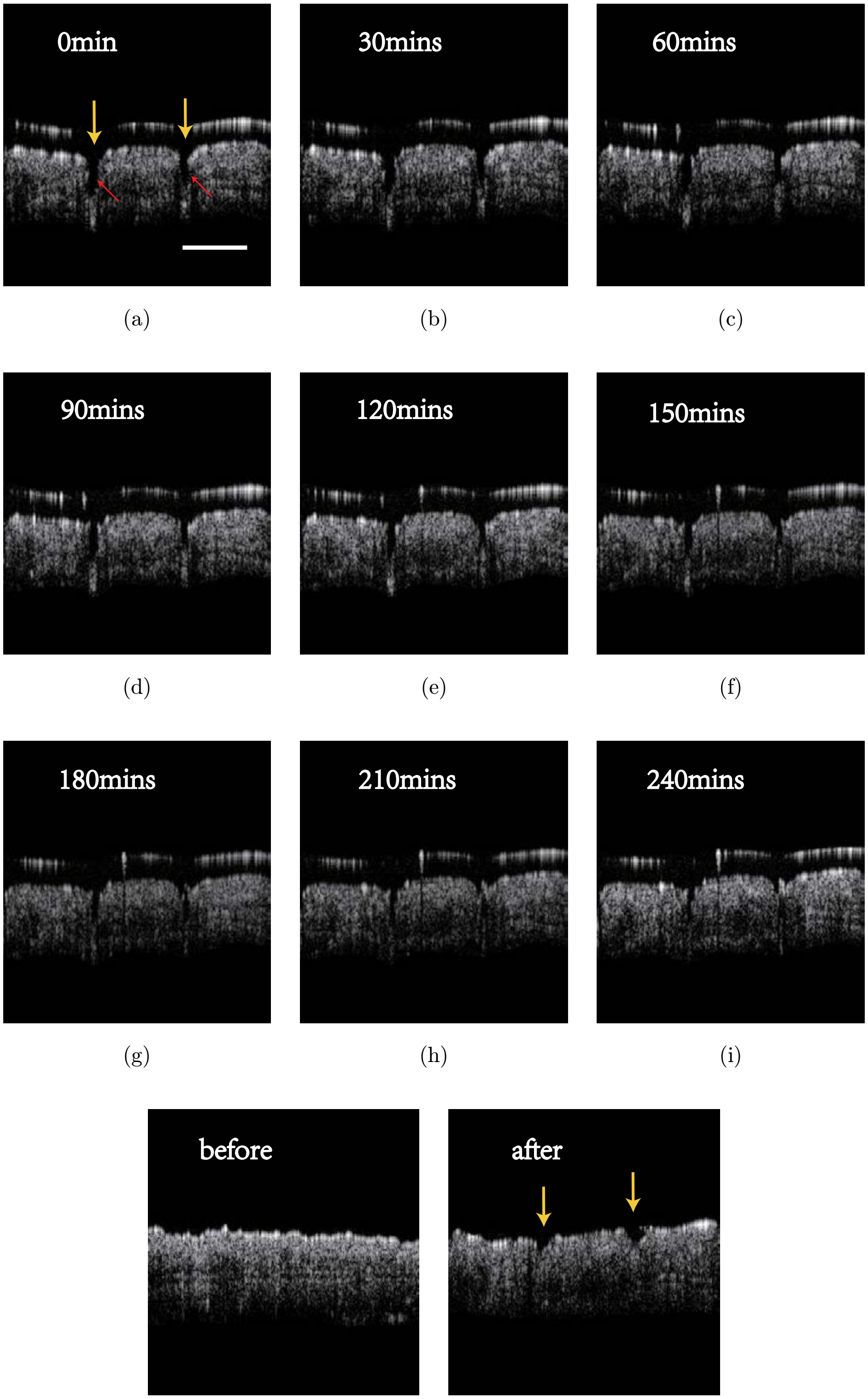

(a) (b) (c)

(d) (e) (f)

(g) (h) (i)

(j) (k)

Fig. 5. OCT images of the dissolving process of PVA/PVP MNs on mouse ear (j) before inserting the microneedle patch on the skin at (a) 0 min, (b) 30 mins, (c) 60 mins, (d) 90 mins, (e) 120 mins, (f) 150 mins, (g) 180 mins, (h) 210 mins, (i) 240 mins and (k) after removing the MN patch. The scale bar and the yellow arrow in (a) represent 1 mm in length and the location where the microneedle is inserted into the skin.

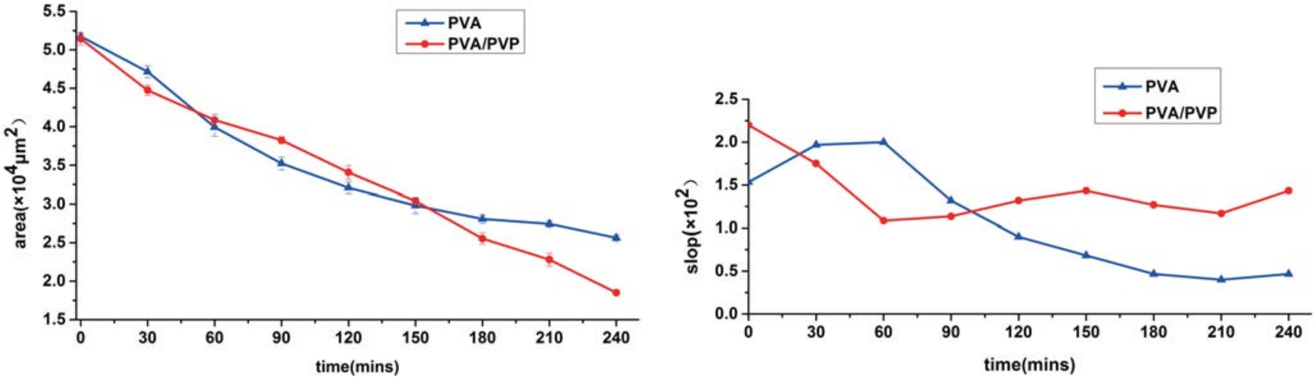

(a) (b)

Fig. 6. (a) Estimated areas of cross-sections of microchannels resulted from PVA MN arrays and PVA/PVP MN arrays as a function of time and (b) The slop of Fig. 6(a).

skin. OCT can thus easily obtain the structural image of MNs changes *in vivo*.

3.3. *Functional imaging after MNs acting on the skin with LSCI*

We evaluate the effect of PVA MNs or PVA/PVP MNs on the skin microvascular with LSCI. Figures 7 and 8 show the microvascular reactivity before and after PVA MNs or PVA/PVP MNs acting on the mouse ears. We collected the images every 5 mins. Corresponding to Figs. 7, 8 and 9 shows the mean perfusion level of the same region. Before the PVA MNs or PVA/PVP MNs acting on the skin (Figs. 7(a) and 8(a)), the color of the ear is shallow and the mean perfusion level of the region

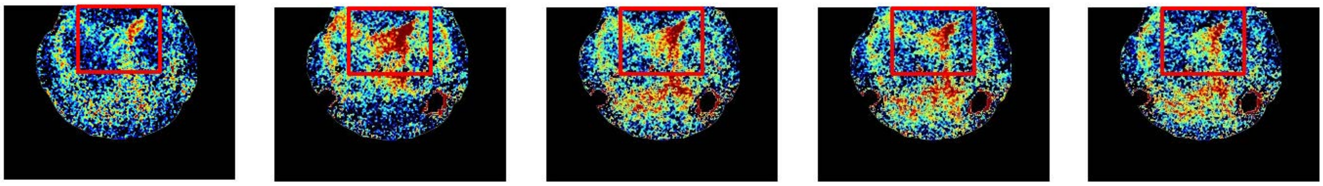

(a) before (b) insert 0 min (c) insert 5 mins (d) insert 10 mins (e) insert 15 mins

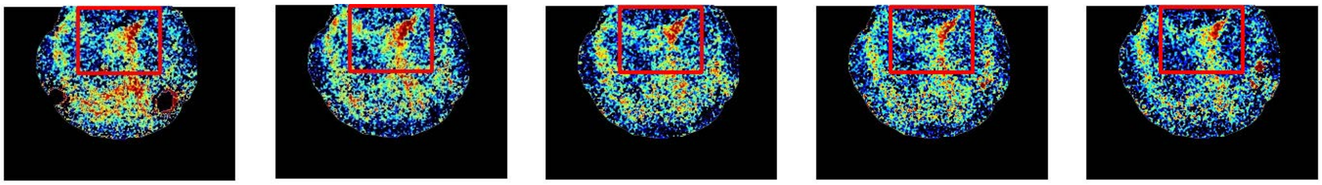

(f) insert 20 mins (g) remove 0 min (h) remove 5 mins (i) remove 10 mins (j) remove 15 mins

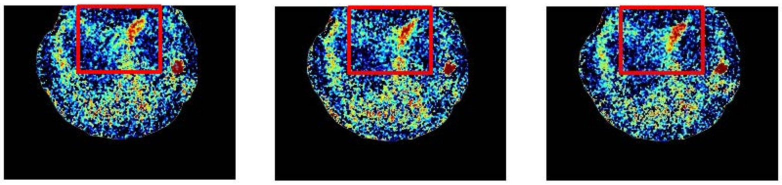

(k) remove 20 mins (l) remove 25 mins (m) remove 30 mins

Fig. 7. Microvascular reactivity: (a) before PVA MNs inserting in the skin of mouse ear, (b) 0 min, (c) 5 mins, (d) 10 mins, (e) 15 mins, (f) 20 mins after inserting PVA MNs into the skin and (g) 0 min, (h) 5 mins, (i) 10 mins, (j) 15 mins, (k) 20 mins, (l) 25 mins and (m) 30 mins after removing PVA MNs.

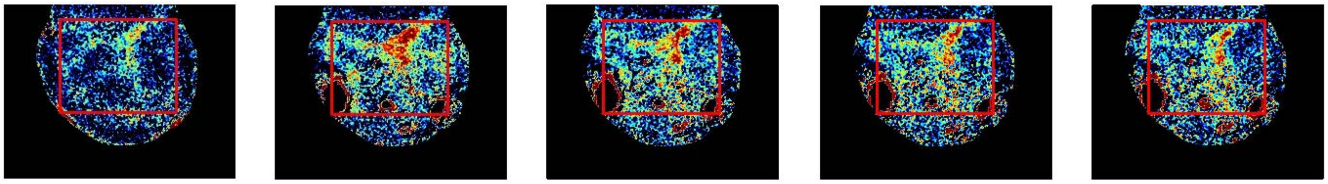

(a) before (b) insert 0 min (c) insert 5 mins (d) insert 10 mins (e) insert 15 mins

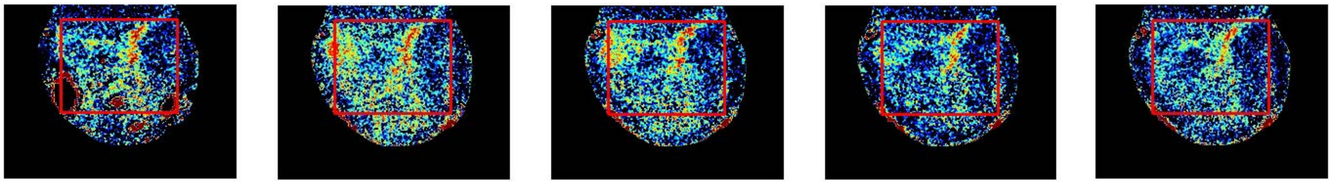

(f) insert 20 mins (g) remove 0 min (h) remove 5 mins (i) remove 10 mins (j) remove 15 mins

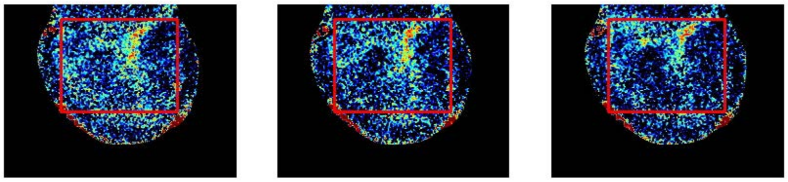

(k) remove 20 mins (l) remove 25 mins (m) remove 30 mins

Fig. 8. Microvascular reactivity: (a) before PVA/PVP MNs inserting in the skin of mouse ear, (b) 0 min, (c) 5 mins, (d) 10 mins, (e) 15 mins, (f) 20 mins after inserting PVA/PVP MNs into the skin, (g) 0 min, (h) 5 mins, (i) 10 mins, (j) 15 mins, (k) 20 mins, (l) 25 mins and (m) 30 mins after removing PVA/PVP MNs.

(in the red box in Figs. 7 and 8) is below 50 or 40 (the part before blue dotted of Fig. 9). After inserting the PVA MNs or PVA/PVP MNs into the skin (Figs. 7(b)–7(f) and Figs. 8(b)–8(f)), the color of the microvascular becomes red which means blood flow becomes faster. The mean perfusion level in Fig. 9 (the part between blue and red dotted line) has a leap at the beginning and then stays at a higher level. After removing the PVA MNs or PVA/PVP MNs from the skin (Figs. 7(g)–7(m) and Figs. 8(g)–8(m)), the velocity of blood flow gradually slows down. It can also be shown from Fig. 9 (the part after red dotted line). The mean perfusion level falls back below 50 or 40 and remains at a lower level. After acting on the skin, both PVA MNs and PVA/PVP MNs will accelerate blood circulation and promote the transfer and absorption of drugs (e.g., insulin) in the blood. After pulling out the MNs for about 30 mins, microcirculation returns to normal state.

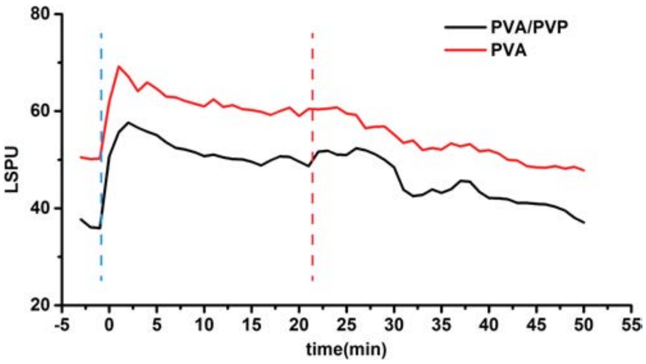

Fig. 9. Mean perfusion level of the interest region as a function of time. The part before blue dotted line indicates the mean perfusion before PVA MNs or PVA/PVP MNs inserting in the skin. The part between blue and red dotted line indicates the mean perfusion after inserting PVA MNs or PVA/PVP MNs into the skin. The part after red dotted line indicates the mean perfusion after removing PVA MNs or PVA/PVP MNs.

3.4. *Transdermal delivery of insulin in balb/c rats*

Healthy balb/c mice were used in this experiment. Figure 10 shows the blood glucose level of mice in four groups, namely, control group (not administrated with any drug), PVA/PVP group (administrated with insulin-loaded PVA/PVP MN arrays), PVA

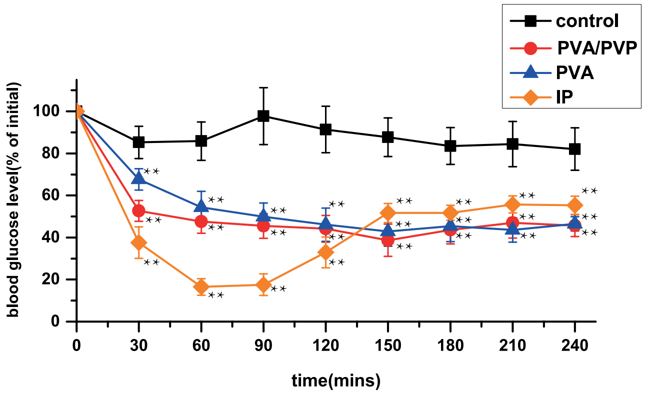

Fig. 10. Blood glucose level as a function of time. Abbreviations: Control, without any drug administration; PVA/PVP, insulin-loaded PVA/PVP MN arrays; PVA, insulin-loaded PVA MN arrays; IP, intraperitoneal injection of insulin. Results are presented as the mean ± S.E. of six experiments.

group (administrated with insulin-loaded PVA MN arrays), and IP group (injected with insulin). The glucose level in control group remained high. Hypoglycemic effect was observed in IP group and in the PVA/PVP MN and PVA MN array groups. The blood glucose levels were significantly lower in the PVA/PVP, PVA, and IP groups than in control ($P < 0.001$) at every time point. A maximum reduction in glucose level was observed 150 mins after insertion of insulin-loaded PVA/PVP MN arrays and PVA MN arrays into the skin. The corresponding maximum reductions in blood glucose levels relative to their initial values were approximately 38.7% and 42.9%. The blood glucose levels remained at a low level thereafter. In IP group, the blood glucose dropped rapidly and reached the lowest percentage of 16.5% at 1 h. Subsequently, the blood glucose rose quickly. Compared with those in the soluble MN array groups, the blood glucose levels in the IP group dropped and then rose rapidly. Moreover, insulin injection possibly results in physical discomfort in this traditional drug delivery system. This result indicates that the insulin loaded in PVA/PVP MN arrays and PVA MN arrays was transmitted into the bloodstream after it was absorbed by the skin. This phenomenon resulted in a gradual reduction in blood sugar, and then the blood glucose level remained at low level as the material dissolves over time. The maximum reduction in blood glucose level after insertion of MNs was higher than that after injection of insulin. Moreover, within the first 30 mins, the blood glucose level dropped more rapidly in PVA/PVP group than in PVA group (PVA/PVP versus PVA at 30 mins $P < 0.001$). This result demonstrated that PVA/PVP MN arrays initially dissolved faster than PVA MN arrays.

In summary, PVA and PVA/PVP soluble MNs were fabricated as a means of loading insulin for transdermal delivery. Dissolution of these two types of MNs was observed *in vivo* by OCT in real time. We also observed the effect of MNs on microcirculation with LSCI. Their dissolution was quantitatively evaluated by calculating the cross-sectional areas of the microchannels in the skin. The estimated cross-sectional areas decreased as MNs dissolved within 4 h. We compared the performance of the different types of MNs with the estimated cross-sectional areas in OCT images and the transdermal delivery of insulin. Moreover, the experimental results show that the soluble MNs offer a potential application in sustained drug release in clinics and improve the penetration efficiency on skin. Generally, OCT can obtain structural image of MNs' changes *in vivo*. LSCI can perform functional imaging of effects of MNs on skin microcirculation. According to the comparison of the administration with different MNs, it gives advice on choosing different types of microneedles for different types of patients.

Acknowledgments

This work was supported by the National Natural Science Foundation of China (Nos. 81571837, 81601534 and 61575067).

References

1. J. G. Llaurado, "Insulin delivery control systems for diabetics," *Int. J. Biomed. Comput.* **14**, 1–3 (1983).
2. Y. Y. Luo, X. Y. Xiong, Y. Tian, Z. L. Li, Y. C. Gong, Y. P. Li, "A review of biodegradable polymeric systems for oral insulin delivery," *Drug Deliv.* **23**, 1–10 (2015).
3. N. Jeandidier, S. Boivin, "Current status and future prospects of parenteral insulin regimens, strategies and delivery systems for diabetes treatment," *Adv. Drug Deliv. Rev.* **35**, 179–198 (1999).
4. V. I. Sevast'Yanov, L. A. Salomatina, E. G. Kuznetsova, N. V. Yakovleva, V. I. Shumakov, "Transdermal insulin delivery systems," *Biomed. Eng.* **37**, 90–94 (2003).
5. M. R. Prausnitz, S. Mitragotri, R. Langer, "Current status and future potential of transdermal drug

delivery," *Nat. Rev. Drug Discov.* **3**, 115–124 (2004).

6. J. D. Bos, M. M. Meinardi, "The 500 Dalton rule for the skin penetration of chemical compounds and drugs," *Exp. Dermatol.* **9**, 165–169 (2000).
7. W. Martanto, S. P. Davis, N. J. Holiday, J. Wang, H. S. Gill, M. R. Prausnitz, "Transdermal delivery of insulin using microneedles *in vivo*," *Pharm. Res.* **21**, 947–952 (2004).
8. J. A. Mikszta, J. B. Alarcon, J. M. Brittingham, D. E. Sutter, R. J. Pettis, N. G. Harvey, "Improved genetic immunization via micromechanical disruption of skin-barrier function and targeted epidermal delivery," *Nat. Med.* **8**, 415–419 (2002).
9. D. G. Koutsonanos, M. D. P. Martin, V. G. Zarnitsyn, S. P. Sullivan, R. W. Compans, M. R. Prausnitz, I. Skountzou, "Transdermal influenza immunization with vaccine-coated microneedle arrays," *PLoS One* **4**, e4773 (2009).
10. M. R. Prausnitz, "Microneedles for transdermal drug delivery," *Adv. Drug Deliv. Rev.* **56**, 581–587 (2004).
11. S. Henry, D. V. Mcallister, M. G. Allen, M. R. Prausnitz, "Microfabricated microneedles: A novel approach to transdermal drug delivery," *J. Pharm. Sci.* **87**, 922–925 (1998).
12. H. S. Gill, M. R. Prausnitz, "Coated microneedles for transdermal delivery," *J. Control. Release.* **117**, 227–237 (2007).
13. M. Wang, L. Hu, C. Xu, "Recent advances in the design of polymeric microneedles for transdermal drug delivery and biosensing," *Lab Chip.* **17**, 1373–1387 (2017).
14. J. H. Park, M. G. Allen, M. R. Prausnitz, "Polymer microneedles for controlled-release drug delivery," *Pharm. Res.* **23**, 1008–1019 (2006).
15. L. Y. Chu, S. O. Choi, M. R. Prausnitz, "Fabrication of dissolving polymer microneedles for controlled drug encapsulation and delivery: Bubble and pedestal microneedle designs," *J. Pharm. Sci.* **99**, 4228–4238 (2010).
16. I. C. Lee, J. S. He, M. T. Tsai, K. C. Lin, "Fabrication of a novel partially dissolving polymer microneedle patch for transdermal drug delivery," *J. Mater. Chem. B* **3**, 276–285 (2015).
17. K. Tsioris, W. K. Raja, E. M. Pritchard, B. Panilaitis, D. L. Kaplan, F. G. Omenetto, "Fabrication of silk microneedles for controlled–release drug delivery," *Adv. Funct. Mater.* **22**, 330–335 (2012).
18. Y. H. Park, K. H. Sang, I. Choi, K. S. Kim, J. Park, N. Choi, B. Kim, J. H. Sung, "Fabrication of degradable carboxymethyl cellulose (CMC) microneedle with laser writing and replica molding process for enhancement of transdermal drug delivery," *Biotechnol. Bioproc. E* **21**, 110–118 (2016).
19. Y. Ito, T. Nakahigashi, N. Yoshimoto, Y. Ueda, N. Hamasaki, K. Takada, "Transdermal insulin application system with dissolving microneedles," *Diabetes. Technol. The.* **14**, 891–899 (2012).
20. S. Lau, J. Fei, H. Liu, W. Chen, R. Liu, "Multilayered pyramidal dissolving microneedle patches with flexible pedestals for improving effective drug delivery," *J. Control. Release.* **265**, 113–119 (2017).
21. D. Liu, B. Yu, G. Jiang, W. Yu, Y. Zhang, B. Xu, "Fabrication of composite microneedles integrated with insulin-loaded $CaCO_3$ microparticles and PVP for transdermal delivery in diabetic rats," *Mater. Sci. Eng. C* **90**, 180–188 (2018).
22. Y. Zhang, G. Jiang, W. Yu, D. Liu, B. Xu, "Microneedles fabricated from alginate and maltose for transdermal delivery of insulin on diabetic rats," *Mater. Sci. Eng. C* **85**, 18–26 (2018).
23. D. Liu, Y. Zhang, G. Jiang, W. Yu, B. Xu, J. Zhu, "Fabrication of dissolving microneedles with thermal-responsive coating for NIR-Triggered transdermal delivery of metformin on diabetic rats," *ACS Biomater. Sci. Eng.* **4**, 1687–1695 (2018).
24. W. Yu, G. Jiang, Y. Zhang, D. Liu, B. Xu, J. Zhou, "Near-infrared light triggered and separable microneedles for transdermal delivery of metformin in diabetic rats," *J. Mater. Chem. B* **5**, 9507–9513 (2017).
25. T. Rattanapak, J. Birchall, K. Young, M. Ishii, I. Meglinski, T. Rades, S. Hook, "Transcutaneous immunization using microneedles and cubosomes: Mechanistic investigations using optical coherence tomography and two-photon microscopy," *J. Control. Release.* **172**, 894–903 (2013).
26. K. Yan, H. Todo, K. Sugibayashi, "Transdermal drug delivery by in-skin electroporation using a microneedle array," *Int. J. Pharm.* **397**, 77–83 (2010).
27. J. Enfield, M. L. O'Connell, K. Lawlor, E. Jonathan, C. O'Mahony, M. Leahy, "*In-vivo* dynamic characterization of microneedle skin penetration using optical coherence tomography," *J. Biomed. Opt.* **15**, 046001 (2010).
28. S. A. Coulman, J. C. Birchall, A. Alex, M. Pearton, B. Hofer, C. O'Mahony, W. Drexler, B. Povazay, "*In vivo*, in situ imaging of microneedle insertion into the skin of human volunteers using optical coherence tomography," *Pharm. Res.* **28**, 66–81 (2011).
29. R. F. Donnelly, M. J. Garland, D. I. Morrow, K. Migalska, T. R. Singh, R. Majithiya, A. D. Woolfson, "Optical coherence tomography is a valuable tool in the study of the effects of microneedle geometry on skin penetration characteristics and in-skin dissolution," *J. Control. Release.* **147**, 333–341 (2010).

30. R. Liu, M. Zhang, C. Jin, "*In vivo* and in situ imaging of controlled-release dissolving silk microneedles into the skin by optical coherence tomography," *J. Biophotonics.* **10**, 870–877 (2017).
31. M. T. Tsai, I. C. Lee, Z. F. Lee, H. L. Liu, C. C. Wang, Y. C. Choia, H. Y. Chou, J. D. Lee, "*In vivo* investigation of temporal effects and drug delivery induced by transdermal microneedles with optical coherence tomography," *Biomed. Opt. Express* **7**, 1865–1876 (2016).
32. D. A. Boas, A. K. Dunn, "Laser speckle contrast imaging in biomedical optics," *J. Biomed. Opt.* **15**, 011109 (2010).
33. K. R. Forrester, J. Tulip, C. Leonard, C. Stewart, R. C. Bray, "A laser speckle imaging technique for measuring tissue perfusion," *IEEE T. Bio-Med. Eng.* **51**, 2074–2084 (2004).
34. J. H. Park, M. G. Allen, M. R. Prausnitz, "Biodegradable polymer microneedles: Fabrication, mechanics and transdermal drug delivery," *J. Control. Release.* **104**, 51–66 (2005).
35. L. Duan, Y. He, R. Zhu, H. Ma, J. Guo, "Development of a spectrum domain 3D optical coherence tomography system," *Chin. J. Lasers* **36**, 2528–2533 (2009).
36. X. Guo, Z. Guo, H. Wei, H. Yang, Y. He, S. Xie, G. Wu, X. Deng, Q. Zhao, L. Li, "*In vivo* comparison of the optical clearing efficacy of optical clearing agents in human skin by quantifying permeability using optical coherence tomography," *Photochem. Photobiol.* **87**, 734–740 (2011).
37. J. Senarathna, A. Rege, N. Li, N. V. Thakor, "Laser speckle contrast imaging: Theory, instrumentation and applications," *IEEE Rev. Biomed. Eng.* **6**, 99–110 (2013).